SIMULTANEOUS RECONSTRUCTION OF TEMPERATURE FIELD AND RADIATIVE PROPERTIES BY INVERSE RADIATION ANALYSIS USING STOCHASTIC PARTICLE SWARM OPTIMIZATION

by

Dong LIU

School of Energy and Power Engineering, Nanjing University of Science and Technology, Nanjing, China

Original scientific paper
DOI:10.2298/TSCI130621053L

Simultaneous reconstruction of temperature field and radiative properties including scattering albedo and extinction coefficient is presented in a 2-D rectangular, absorbing, emitting, and isotropically scattering gray medium from the knowledge of the exit radiative intensities received by charge-coupled device cameras at boundary surfaces. The inverse problem is formulated as a non-linear optimization problem and solved by stochastic particle swarm optimization. The effects of particle swarm size, generation number, measurement errors, and optical thickness on the accuracy of the estimation, and computing time were investigated and the results show that the temperature field and radiative properties can be reconstructed well for the exact and noisy data, but radiative properties are harder to obtain than temperature field. Moreover, the extinction coefficient is more difficult to reconstruct than scattering albedo.

Key words: *simultaneous reconstruction, temperature field, radiative properties, particle swarm optimization*

Introduction

The inverse radiation analysis in the participating medium has many applications, such as the determination of the radiative properties of the medium, the estimation of the temperature distribution, and so on. A comprehensive review of inverse radiation problems has been given by McCormick [1]. Lots of work has been reported on the estimation of temperature field or source term distribution under the assumption of known radiative properties of the medium, such as the work of Li and Ozisik [2], Siewert [3, 4], Li [5-7], Liu *et al.* [8, 10], Liu and Tan [9], Zhou *et al.* [11], Liu *et al.* [12, 13], Wang *et al.* [14], and Dong *et al.* [15, 16]. Simultaneous estimation of temperature profile and properties of boundary surface were also conducted by some researchers, *e. g.*, Li and Ozisik [17] presented a method for simultaneous estimation of the unknown temperature distribution and the diffuse surface reflectivity in the participating medium, and Liu *et al.* [18, 19] conducted the simultaneous identification of the temperature profile or sources and the boundary emissivities in 1-D semitransparent medium.

Simultaneous estimation of temperature field and the radiative properties of the participating medium or soot volume fraction of flame have aroused many interests of researchers. Liu [20] carried out the simultaneous identification of temperature profile and uniform absorption coefficient in 1-D semitransparent medium. Zhou *et al.* [21] conducted simultaneous estimation

Author's e-mail: dongliu@njust.edu.cn

of temperature, absorption and scattering coefficient profile in 1-D medium from the boundary intensity and boundary temperature profiles. Snelling *et al.* [22] developed a multi-wave-length flame emission technique for high spatial resolution determination of soot temperature and soot volume fraction in axisymmetric laminar diffusion flames. Ayranci *et al.* [23] determined soot temperature, volume fraction and refractive index from flame emission spectrometry for an optically thin axisymmetric flame. Zhou and Han [24] reconstructed temperature distribution, absorptivity of wall surface and absorption coefficient of medium in a 2-D furnace system filled with gray emitting/absorption medium. Lou *et al.* [25] used flame images to obtain the flame emissivity and the uniform radiative properties of the particulate media in pulverized-coal-fired boiler furnaces by modified Tikhonov regularization method and iteration algorithm. Liu *et al.* [26] presented inverse radiation analysis for simultaneous estimation of temperature field and uniform radiative properties in participating medium using LSQR method and 2-D searching, and also used charge-coupled device (CCD) cameras to simultaneously measure 3-D soot temperature and volume fraction fields in axisymmetric or asymmetric small unconfined flames with optically thin medium [27, 28]. Lou *et al.* [29] reported simultaneous measurement of temperature field, uniform absorption coefficient of medium and emissivity of wall surface by inverse analysis. Wang *et al.* [30] reconstructed 2-D temperature and particle concentration distribution from the image of the pulverized coal flame simultaneously using optimization method by ignoring scattering of the medium, but in the large pulverized coal-fired furnace, the scattering should not be neglected in most space of the furnace [31]. In the real situation, the distribution of radiative properties is generally non-uniform, but simultaneous estimation of 2-D or 3-D temperature distribution and non-uniform radiative properties is still a formidable work. Therefore, the available studies of simultaneous estimation of 2-D temperature distribution and radiative properties in participating medium are only limited to the uniform radiative properties [24-26, 29]. Lou *et al.* [29] and Lou and Zhou [32] have reported that using the uniform radiative properties to reconstruct the temperature distribution in the inhomogeneous system may take some errors, and have proved that the maximum reconstruction error of temperature is less than 6%.

In recent years, as an alternative to gradient-based methods, genetic algorithm and particle swarm optimization (PSO) algorithm have increasingly been applied to the inverse radiation problem [33-42]. In the present study, we used stochastic PSO for simultaneous reconstruction of temperature field and radiative properties including scattering albedo and extinction coefficients with different kinds of optical thicknesses in a large 2-D rectangular, absorbing, emitting, and isotropically scattering medium from the knowledge of the exit radiative intensities received by CCD cameras at the boundary surfaces. The effects of particle swarm size, generation number, measurement errors, and optical thickness on the accuracy of the estimation, and computing time were investigated.

Analysis

Direct problem

For the participating medium the radiative heat transfer equation can be written [43]:

$$\frac{\mathrm{d}I_\lambda}{\mathrm{d}\tau_\lambda} + I_\lambda = S_\lambda(\tau_\lambda, \vec{\mathrm{s}}) \tag{1}$$

with

$$S_\lambda(\tau_\lambda, \vec{\mathrm{s}}) = (1-\omega)I_{\mathrm{b}\lambda} + \frac{\omega}{4\pi}\int_{4\pi} I_\lambda(\vec{\mathrm{s}}_i)\Phi_\lambda(\vec{\mathrm{s}}_i, \vec{\mathrm{s}})\mathrm{d}\Omega_i$$

where $\vec{s}$ is a unit local direction vector, S – the local radiative source, ω – the local scattering albedo, τ_λ – the optical thickness, Φ_λ – the scattering phase function, and Ω – the solid angle.

Considering the following system as shown in fig. 1, integration of eq. (1) over a single radiation ray in one volume element from τ_{in} to τ_{out} results in:

$$I_\lambda(\tau_{\text{out}}) = I_\lambda(\tau_{\text{in}})\text{e}^{-\tau} + \int_{\tau_{\text{in}}}^{\tau_{\text{out}}} S_\lambda(\tau'_\lambda, \vec{s})\text{e}^{-(\tau_{\text{out}}-\tau'_\lambda)}\text{d}\tau'_\lambda \tag{2}$$

where $\tau = \tau_{\text{out}} - \tau_{\text{in}}$.

It was pointed out by Lockwood and Shah [44] that the in-scattering term is zero for gas flames, negligible for oil flames, while for coal flames it is often acceptable to ignore it with the effect of particle scattering largely being accounted for by the out-scattering term. This approximation was later utilized in numerical simulations for coal-fired utility boilers [45, 46] and in their studies comparisons between numerical simulation and measurements were also carried out. The temperature and radiative properties are assumed to be uniform within one volume element. Based on the previous considerations, eq. (2) can be simplified to:

$$I_\lambda(\tau_{\text{out}}) = I_\lambda(\tau_{\text{in}})\text{e}^{-\tau} + (1-\omega)I_{\text{b}\lambda}(1-\text{e}^{-\tau}) \tag{3}$$

Considering the whole ray j from one side of the system to the CCD camera, based on eq. (3) the intensity received by CCD camera can be:

$$\begin{aligned} I_{\lambda j} = {} & I_{\lambda 0}\text{e}^{-(\tau_1+\cdots+\tau_S)} + (1-\omega_1)I_{\text{b}\lambda 1}(1-\text{e}^{-\tau_1})\text{e}^{-(\tau_2+\cdots+\tau_S)} + \\ & + \cdots + (1-\omega_s)I_{\text{b}\lambda s}(1-\text{e}^{-\tau_s})\text{e}^{-(\tau_{s+1}+\cdots+\tau_S)} + \cdots \\ & + (1-\omega_S)I_{\text{b}\lambda S}(1-\text{e}^{-\tau_S}) \end{aligned} \tag{4}$$

where s is the s^{th} volume element of ray traversing and S – the total volume element number of ray traversing.

If at the CCD camera location, the discrete direction number is assumed to be M, the following equations can be obtained based on eq. (4):

$$\begin{gathered} f_1(I_{\text{b}\lambda 1}, I_{\text{b}\lambda 2}, \cdots, I_{\text{b}\lambda N}) = I_{\lambda 1} \\ \vdots \\ f_j(I_{\text{b}\lambda 1}, I_{\text{b}\lambda 2}, \cdots, I_{\text{b}\lambda N}) = I_{\lambda j} \\ \vdots \\ f_M(I_{\text{b}\lambda 1}, I_{\text{b}\lambda 2}, \cdots, I_{\text{b}\lambda N}) = I_{\lambda M} \end{gathered} \tag{5}$$

where N is the total number of volume element.

Usually in the high temperature furnace the water-wall temperatures are much lower than inner medium temperatures, rewrite eq. (5) to the matrix form:

$$[\text{A}]\,\vec{\text{I}}_{\text{b}} = \vec{\text{I}}_{\text{CCD}} \tag{6}$$

where [A] is the coefficient matrix, $\vec{\text{I}}_{\text{b}}$ – the unknown blackbody intensity vector from which the temperatures can be obtained, and $\vec{\text{I}}_{\text{CCD}}$ – the monochromatic intensity vector received by CCD cameras, which is the input data in the reconstruction process.

In the direct problem, for the known temperature field and radiative properties including scattering albedo and extinction coefficient (absorption and scattering coefficients), the intensities received by CCD cameras can be obtained by eq. (6).

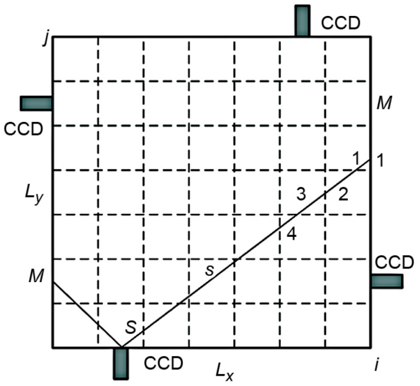

Figure 1. The 2-D rectangular enclosure with CCD cameras

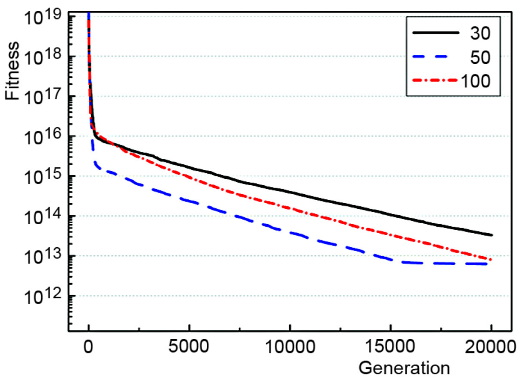

Figure 2. Effect of particle swarm size on the fitness of objective function

Inverse problem

For the inverse problem, the temperature field and radiative properties are regarded as unknown and the intensities received by CCD cameras are known. The temperature field and radiative properties can be reconstructed simultaneously by using the intensities received by CCD cameras.

Simultaneous reconstruction of temperature field and radiative properties including scattering albedo and extinction coefficient is a non-linear optimization problem. Stochastic PSO was used to directly solve this non-linear optimization problem. The simple principle of stochastic PSO algorithm was described as follows [39, 42]. Each individual in particle swarm, referred to as a particle. Every particle moves its position in search domain and updates its velocity according to its own flying experience and neighbor's flying experience, aiming at a better position for itself and a global fitness.

At generation t, the i^{th} particle $X_i(t)$ can be described as $X_i(t) = [x_{i1}(t),\dots, x_{ij}(t),\dots, x_{in}(t)]^T$, the velocity is described as $V_i(t) = [v_{i1}(t),\dots, v_{ij}(t),\dots, v_{in}(t)]$T, the individual best position is expressed as $P_i(t) = [p_{i1}(t),\dots, p_{ij}(t),\dots, p_{in}(t)]^T$, and the global best position of the swarm is expressed as $P_g(t) = [p_{g1}(t),\dots, p_{gj}(t),\dots, p_{gn}(t)]^T$, where $x_{ij}(t)$ is the position of the i^{th} particle with the j^{th} dimension, *i. e.* the value of the j^{th} optimized parameter in the i^{th} candidate solution, $v_{ij}(t)$ – the velocity of the i^{th} particle with j^{th} dimension, $p_{ij}(t)$ – the local best position of the i^{th} particle with j^{th} dimension, $p_{gj}(t)$ – the best of all positions with j^{th} dimension, and n – the number of optimization variables.

For the stochastic PSO, the velocity and position of the particle update according to the following equations:

$$V_i(t+1) = c_1 r_1 [P_i(t) - X_i(t)] + c_2 r_2 [P_g(t) - X_i(t)] \tag{7}$$

$$X_i(t+1) = X_i(t) + V_i(t+1) \tag{8}$$

where, c_1, c_2 are the acceleration coefficients, r_1, r_2 – the uniform random variables in the range [0, 1].

The objective function is defined:

$$f\left(T, \text{albedo}, \kappa_{\text{ext}}\right) = \left\| A\vec{\mathrm{I}}_{\mathrm{b}} - \vec{\mathrm{I}}_{\mathrm{CCD}} \right\|^2 + \mu\,\Psi(T) \tag{9}$$

where $\Psi(T)$ is the smoothing function of temperature field, and μ – the weight coefficient.

Results and discussion

As shown in fig. 1, the size of 2-D rectangular enclosure was 10 m × 10 m. The viewing angle of the CCD camera was assumed to be 120° and for the high temperature system, the walls could be assumed to be black and cold for simplicity. The wavelength used here was 700 nm, which was in the visible wavelength range. For the non-linear optimization problem, more discrete volume elements are divided, more computing time is consumed. Considering the computing time and the practical use, the discrete volume elements of system were assumed to be 5 × 5 in order to reduce the computing time and complexity. In the practical use, when the coarse temperature field is obtained, the main features of the system are obtained, and then more delicate temperature distribution can be deduced by using 2-D interpolation, which already has matured algorithms. The discrete direction number was 25 for each CCD camera.

The measured intensities received by CCD cameras were simulated by adding random errors of normal distribution with zero average value and mean square deviation σ to the exact intensities which can be obtained from the direct problem:

$$I_{\text{measured},j} = (\mu + \sigma\xi)I_j + I_j \tag{10}$$

where $I_{\text{measured},j}$ is the element of the simulated measured intensity vector and I_j – the element of the exact intensity vector. Average value μ equals zero, ξ – a random variable of standard normal distribution and the probability lying in the range of $-2.576 < \xi < 2.576$ is 99%. $j = 1, 2, \ldots, M$.

An assumed temperature field and radiative properties including scattering albedo and extinction coefficient were provided for testing the method developed here. The assumed temperature field was shown in fig. 4. The scattering albedo was assumed to be 0.5. Two kinds of extinction coefficients were assumed to be (a) 0.2 m^{-1} and (b) 0.6 m^{-1}. The corresponding optical thicknesses τ were (a) 2.0 and (b) 6.0. The assumed optical thicknesses were all optically thick.

The relative error of the temperature in each volume element is:

$$E_{\text{rel},i} = \frac{100\left|T_i^{\text{recon}} - T_i^{\text{exact}}\right|}{T_i^{\text{exact}}} \tag{11}$$

where T_i^{recon} and T_i^{exact} are reconstructed and exact temperature, respectively, $i = 1, 2, \ldots, N$.

The maximum, mean, and minimum relative errors of temperature distribution are:

$$\max = \text{maxmimum } (E_{\text{rel,i}}),\ i = 1, 2, ..., N, \qquad \text{mean} = \sum_{i=1}^{N} \frac{E_{\text{rel,i}}}{N}, \qquad \min = \text{minimum } (E_{\text{rel,i}}),\quad i = 1, 2, ..., N \tag{12}$$

Case 1

In this case, the scattering albedo and extinction coefficient are assumed to be 0.5 and 0.2 m^{-1}. The optical thickness is 2.0. The searching spaces are (1576 K, 1800 K) for temperature, (0.1, 0.9) for scattering albedo, and (0.1 m^{-1}, 0.8 m^{-1}) for extinction coefficient.

Effect of particle swarm size on the fitness of objective function

The effect of particle swarm size on fitness of objective function was examined. Three kinds of swarm size were used, *i. e.*, 30, 50, and 100, as shown in fig. 2. No measurement errors were considered here. The fitness of objective function was the lowest for swarm size 50 in the same generation number. In the generation 20000, the fitnesses of swarm size 50 and 100 are almost the same and it also be noticed from the tendency that after generation 20000 the fitness of swarm size 100 will decrease lower than that of swarm size 50. The swarm size 50 seems the best candidate of three kinds of swarm sizes before generation 20000. Moreover, larger swarm size is used, more computing time is consumed.

Effects of swarm size and generation on the reconstruction accuracy of radiative properties

Effects of swarm size and generation on the reconstruction accuracy of radiative properties were checked, as shown in fig. 3. The measurement errors were assumed to be zero here. For all three kinds of swarm sizes, the reconstruction accuracy of albedo and extinction coefficient increases with the generation. For the scattering albedo reconstruction, before generation 10000 the performances of swarm size 50 and 100 are almost the same, better than that of swarm size 30, and after generation 10000, there are no obvious differences for three kinds of swarm sizes. For the extinction coefficient reconstruction, before generation 15000 the results from swarm size 50 are best, and after generation 15000, there are no obvious differences for three kinds of swarm sizes. In the generation 10000, albedo and extinction coefficient can be reconstructed accurately. Computing time increases linearly with the generation for each swarm size. For the same generation, the computing time increases with the swarm size.

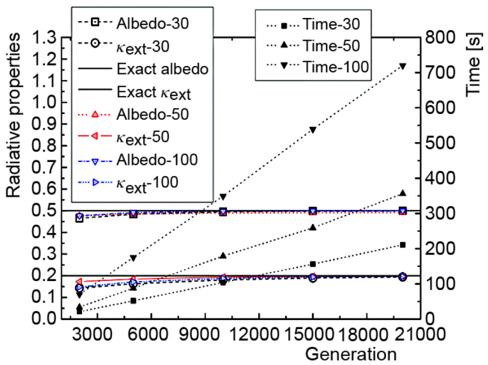

Figure 3. Effect of swarm size and generation on the reconstruction accuracy of radiative properties

Effect of generation on the reconstruction accuracy of temperature field

Measurement errors were assumed to be zero here. It was found that all the three kinds of swarm sizes can obtain satisfying reconstructed temperature field. Particle swarm size 30 was used for examining the effect of generation on the reconstruction accuracy of temperature field for less computing time. The results are shown in fig. 4. The reconstruction accuracy of temperature field increases with the generation. For the generation 10000, the reconstructed temperature field agrees well with the assumed one.

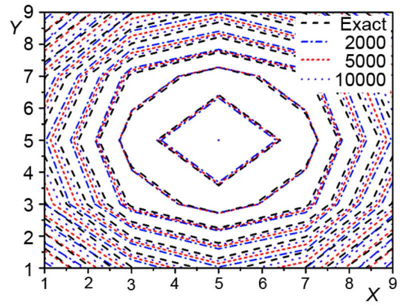

Figure 4. Effect of generation on the reconstruction accuracy of temperature field with swarm size 30

Effect of measurement errors on the reconstruction accuracy of radiative properties

Effect of measurement errors on the reconstruction accuracy of radiative properties was examined. Swarm size 50 and generation 15000 were used here. As shown in fig. 5, it was seen that the albedo and extinction coefficient can be reconstructed well under different measurement errors. The measurement errors can affect the reconstruction accuracy but the relative errors can be maintained at a certain level and did not increase fast with the measurement errors. The reconstruction relative errors of extinction coefficient were larger than those of albedo for most of measurement errors, which indicated that extinction coefficient reconstruction was more sensitive to measurement errors than scattering albedo reconstruction.

Effect of measurement errors on the reconstruction accuracy of temperature field

Swarm size 50 and generation 15000 was used here. From fig. 6, it was noticed that the temperature field can be reconstructed well under different measurement errors. The reconstruction relative errors can be maintained at a low level and did not increase fast with the measurement errors. The reconstruction accuracy of temperature field was better than that of radiative properties, which demonstrated the temperature field was easier to be reconstructed than radiative properties.

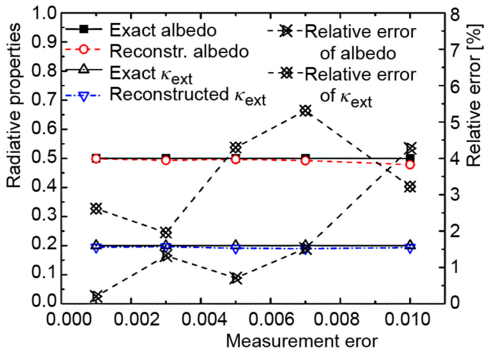

Figure 5. Effect of measurement errors on the reconstruction accuracy of radiative properties for optical thickness 2.0

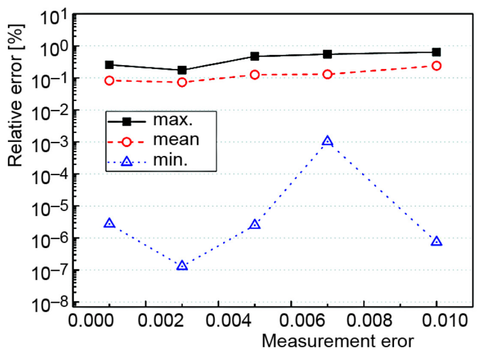

Figure 6. Effect of measurement errors on the reconstruction accuracy of temperature field for optical thickness 2.0

Case 2

In this case, the scattering albedo and extinction coefficient are assumed to be 0.5 and 0.6 m^{-1}. The optical thickness is 6.0. The searching spaces are 1576 K, 1800 K for temperature, 0.1, 0.9 for scattering albedo, and 0.1 m^{-1}, 0.8 m^{-1} for extinction coefficient.

Effects of measurement errors and generation on the reconstruction accuracy of radiative properties

During calculations, it was found that accurate radiative properties can be obtained after generation 50000, so from the discussion of Chapter *Effect of particle swarm size on the fitness of objective function*, particle swarm size 30 was used here for saving computing time. The reconstructed radiative properties with generation 70000 under different measurement errors were shown in fig. 7. Comparing fig. 7 with fig. 3, as the measurement errors are zero, the reconstructed results with optical thickness 6.0 were much worse than those with optical thickness 2.0, which may be due to the less radiative information received by CCD cameras for larger optical thickness. With measurement errors of σ = 0.01, from optical thickness 2.0-6.0 the extinction coefficient reconstruction relative error increases largely, but the albedo reconstruction relative error was similar.

The variations of reconstructed albedo and extinction coefficient with generation under measurement error σ = 0.01 were shown in fig. 8. It was found that the albedo can be reconstructed well in and after generation 5000, but extinction coefficient can only be reconstructed with reasonable error in generation 70000, which implied that the extinction coefficient was more difficult to reconstruct than the scattering albedo.

The computing time is 726 second of generation 70000 and much longer than that for optical thickness 2.0. More time is needed to search for accurate radiative properties (extinction coefficient) when the optical thickness increases.

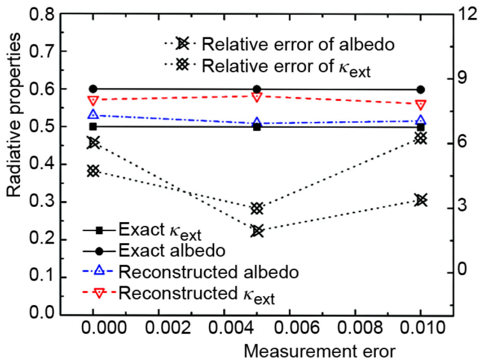

Figure 7. Effect of measurement errors on the reconstruction accuracy of radiative properties for optical thickness 6.0

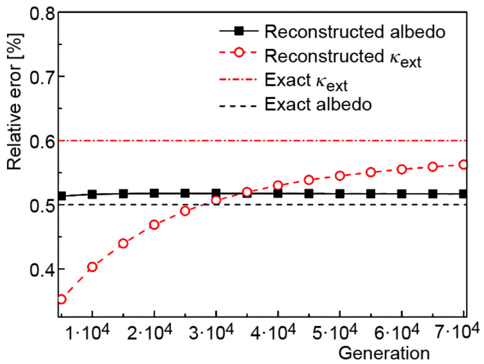

Figure 8. Variations of reconstructed radiative properties with generation under σ = 0.01 for optical thickness 6.0

Effects of measurement errors and generation on the reconstruction accuracy of temperature field

The relative errors of reconstructed temperature fields with generation 70000 under different measurement errors with optical thickness 6.0 were shown in fig. 9. It can be seen that temperature fields can be reconstructed well under different measurement errors. The maximum and mean relative errors do not vary much for different measurement errors, which indicates that the stochastic PSO has anti-error characteristic.

Figure 10 shows the variations of relative errors of reconstructed temperature fields with generation under measurement error σ = 0.01 for optical thickness 6.0. The maximum and mean relative errors decrease with the generation, and the minimum relative error does not vary much with the generation. As the generation is 30000, the maximum reconstruction relative error of temperature field is 1.88% which is satisfying, and also from fig. 8 the albedo is reconstructed well. But the extinction coefficient cannot be reconstructed well in generation 30000. The computing time is about 313 second for generation 30000. All the calculations were carried out on the laptop with an Intel Core 2 Duo CPU 2.40 GHz processor and 2 GB memory.

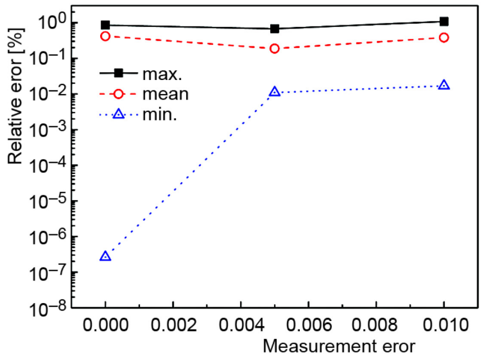

Figure 9. Effect of measurement errors on the reconstruction accuracy of temperature field for optical thickness 6.0

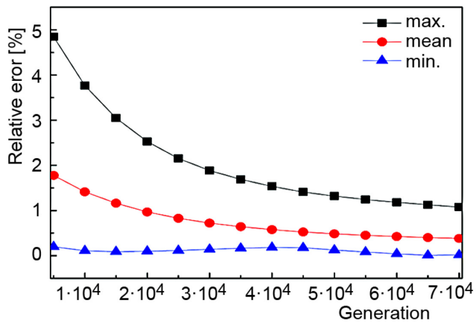

Figure 10. Variations of relative errors of reconstructed temperatures with generation under σ = 0.01 for optical thickness 6.0

Conclusions

This paper presents simultaneous reconstruction of temperature field and radiative properties including scattering albedo and extinction coefficient in a 2-D rectangular, absorbing, emitting, and scattering gray medium from the knowledge of the exit radiative energy received by CCD cameras at boundary surfaces. The inverse problem is formulated as a non-linear optimization problem and solved by stochastic PSO. Two kinds of optical thicknesses were tested. The effects of particle swarm size, generation number, measurement errors on the accuracy of the estimation were examined. The results show that the temperature field and radiative properties can be reconstructed well for the exact and noisy data. Radiative properties are harder to obtain than temperature field. Moreover, the extinction coefficient is more difficult to reconstruct than scattering albedo.

Acknowledgments

This work was supported by the National Natural Science Foundation of China (51306091), the Jiangsu Provincial Natural Science Foundation of China (BK20130758) and the Fundamental Research Funds for the Central Universities (No. 30920140111005).

Nomenclature

A – coefficient matrix, [–]
I – radiation intensity, [Wm^{-3}sr^{-1}]
$\vec{\mathrm{I}}_{\mathrm{CCD}}$ – monochromatic intensity vector, [–]
I_{b} – blackbody intensity vector, [–]
i – number of volume elements on the x side, [–]
j – number of volume elements on the y side, [–]
Lx – length of x side, [m]
Ly – length of y side, [m]
M – discrete direction number, [–]
n – number of optimization variables, [–]
p – local best position of particle, [–]
p_g – best of all positions, [–]
S – total volume element number of ray traversing, [–]
s – s^{th} volume element of ray traversing, [–]
T – temperature, [K]
t – generation, [–]
v – velocity of particle, [–]
x – position of particle, [–]

Greek symbols

κ – coefficient, [m^{-1}]
λ – wavelength, [m]
ξ – random variable of standard normal distribution, [–]
σ – measurement error
τ – optical thickness, [–]
ω – local scattering albedo, [–]
Φ – scattering phase function, [sr^{-1}]
Ψ – smoothing function of temperature field, [–]
Ω – solid angle, [sr]

Subscripts

b – blackbody value
ext – extinction
in – entry point of volume boundary
out – out point of volume boundary

References

[1] McCormick, N. J., Inverse Radiative Transfer Problems: a Review, *Nuclear Science and Engineering, 112* (1992), 3, pp. 185-198
[2] Li, H. Y., Ozisik, M. N., Identification of the Temperature Profile in an Absorbing, Emitting, and Isotropically Scattering Medium by Inverse Analysis, *J. Heat Transfer*, *114* (1992), 4, pp. 1060-1063
[3] Siewert, C. E., An Inverse Source Problem in Radiation Transfer, *JQSRT*, *50* (1993), 6, pp. 603-609
[4] Siewert, C. E., A Radiative-Transfer Inverse-Source Problem for f Sphere, *JQSRT*, *52* (1994), 2, pp. 157-160
[5] Li, H.-Y., Estimation of the Temperature Profile in a Cylindrical Medium by Inverse Analysis, *JQSRT*, *52* (1994), 6, pp. 755-764
[6] Li, H.-Y., Inverse Radiation Problem in Two-Dimensional Rectangular Media. *J. Thermophys. Heat Transfer*, *11* (1997), 4, pp. 556-561
[7] Li, H.-Y., A Two-Dimensional Cylindrical Inverse Source Problem in Radiative Transfer, *JQSRT*, *69* (2001), 4, pp. 403-414
[8] Liu, L.-H., *et al.*, Inverse Radiation Problem of Temperature Field in Three-Dimensional Rectangular Furnaces, *Int. Comm. Heat Mass Transfer*, *26* (1999), 2, pp. 239-248
[9] Liu, L. H., Tan, H. P., Inverse Radiation Problem in Three-Dimensional Complicated Geometric Systems with Opaque Boundaries, *JQSRT*, *68* (2001), 5, pp. 559-573
[10] Liu, L.-H., *et al.*, Inverse Radiation Problem of Source Term in Three-Dimensional Complicated Geometric Semitransparent Media, *Int. J. Therm. Sci.*, *40* (2001), 6, pp. 528-538
[11] Zhou, H.-C., *et al.*, Visualization of Three-Dimensional Temperature Distributions in a Large-Scale Furnace via Regularized Reconstruction from Radiative Energy Images: Numerical Studies, *JQSRT*, *72* (2002), 4, pp. 361-383
[12] Liu, D., *et al.*, Inverse Radiation Problem of Temperature Field in Three-Dimensional Rectangular Enclosure Containing Inhomogeneous, Anisotropically Scattering Media, *Int. J. Heat Mass Transfer*, *51* (2008), 13-14, pp. 3434-3441
[13] Liu, D., *et al.*, Noncontact Temperature Measurement by Means of CCD Cameras in a Participating Medium, *Optics Letters*, *33* (2008), 5, pp. 422-424
[14] Wang, F., *et al.*, Efficient Inverse Radiation Analysis of Temperature Distribution in Participating Medium Based on Backward Monte Carlo Method, *JQSRT*, *109* (2008), 12-13, pp. 2171-2181
[15] Dong, L., *et al.*, Simulation Study on Reconstruction Model of Three-Dimensional Temperature Distribution within Visible Range in Furnace, *Chinese Physics B, 17* (2008), 4, pp. 1312-1317
[16] Dong, L., *et al.*, Fast Reconstruction of Two-Dimensional Temperature Distribution in Participating Medium, *Acta Phys. Sin., 57* (2008), 8, pp. 4812-4816
[17] Li, H. Y., Ozisik, M. N., Inverse Radiation Problem for Simultaneous Estimation of Temperature Profile and Surface Reflectivity, *J. Thermophys. Heat Transfer*, *7* (1993), 1, pp. 88-93
[18] Liu, L. H., *et al.*, Simultaneous Identification of Temperature Profile and Wall Emissivities in One-Dimensional Semitransparent Medium by Inverse Radiation Analysis, *Numerical Heat Transfer, Part A*, *36* (1999), 5, pp. 511-525
[19] Liu, L. H., *et al.*, Inverse Radiation Problem of Sources and Emissivities in One-Dimensional Semitransparent Media, *Int. J. Heat Mass Transfer, 44* (2001), 1, pp. 63-72
[20] Liu, L. H., Simultaneous Identification of Temperature Profile and Absorption Coefficient in One-Dimensional Semitransparent Medium by Inverse Radiation Analysis, *Int. Comm. Heat Mass Transfer*, *27* (2000), 5, pp. 635-643

[21] Zhou, H. C., *et al.*, An Inverse Radiative Transfer Problem of Simultaneously Estimating Profiles of Temperature and Radiative Parameters from Boundary Intensity and Temperature Measurements, *JQSRT*, *74* (2002), 5, pp. 605-620

[22] Snelling, D. R., *et al.*, Spectrally Resolved Measurement of Flame Radiation to Determine Soot Temperature and Concentration, *AIAA Journal*, *40* (2002), 9, pp. 1789-1795

[23] Ayranci, I., *et al.*, Determination of Soot Temperature, Volume Fraction and Refractive Index from Flame Emission Spectrometry, *JQSRT*, *104* (2007), 2, pp. 266-276

[24] Zhou, H. C., Han, S. D., Simultaneous Reconstruction of Temperature Distribution, Absorptivity of Wall Surface and Absorption Coefficient of Medium in a 2-D Furnace System, *Int. J. Heat Mass Transfer*, *46* (2003), 14, pp. 2645-2653

[25] Lou, C., *et al.*, Measurements of the Flame Emissivity and Radiative Properties of Particulate Medium in Pulverized-Coal-Fired Boiler Furnaces by Image Processing of Visible Radiation, *Proceedings of the Combustion Institute*, *31* (2007), 2, pp. 2771-2778

[26] Liu, D., *et al.*, Inverse Radiation Analysis of Simultaneous Estimation of Temperature Field and Radiative Properties in a Two-Dimensional Participating Medium, *Int. J. Heat Mass Transfer*, *53* (2010), 21-22, pp. 4474-4481

[27] Liu, D., *et al.*, Simultaneous Measurement of Three-Dimensional Soot Temperature and Volume Fraction Fields in Axisymmetric or Asymmetric Small Unconfined Flames with CCD Cameras, *J. Heat Transfer*, *132* (2010), 6, pp. 061202-061208

[28] Yan, J.-H, *et al.*, Simultaneous Experimental Reconstruction of Three-Dimensional Flame Soot Temperature and Volume Fraction Distributions, *Acta Phys. Sin., 60* (2011), 6, pp. 060701-060708

[29] Lou, C., *et al.*, Experimental Investigation on Simultaneous Measurement of Temperature Distributions and Radiative Properties in an Oil-Fired Tunnel Furnace by Radiation Analysis, *Int. J. Heat Mass Transfer, 54* (2011), 1-3, pp. 1-8

[30] Wang, F., *et al.*, Simultaneous Measurements of Two-Dimensional Temperature and Particle Concentration Distribution from the Image of the Pulverized Coal Flame, *Fuel*, *89* (2010), 1, pp. 202-211

[31] Liu, D., *et al.*, On the Treatment of Scattering for Three-Dimensional Temperature Distribution Reconstruction Accuracy in Participating Medium, *Int. J. Heat Mass Transfer*, *54* (2010), 7-8, pp. 1684-1687

[32] Lou, C., Zhou, H. C., Assessment of Regularized Reconstruction of Three-Dimensional Temperature Distributions in Large-Scale Furnaces, *Numerical Heat Transfer, Part B*, *53* (2008), 6, pp. 555-567

[33] Li, H. Y., Yang, C. Y., A Genetic Algorithm for Inverse Radiation Problems, *Int. J. Heat Mass Transfer*, *40* (1997), 7, pp. 1545-1549

[34] Kim, K. W., *et al.*, Estimation of Emissivities in a Two-Dimensional Irregular Geometry by Inverse Radiation Analysis Using Hybrid Genetic Algorithm, *JQSRT*, *87* (2004), 1, pp. 1-14

[35] Kim, K. W., Baek, S. W., Inverse Surface Radiation Analysis in an Axisymmetric Cylindrical Enclosure Using a Hybrid Genetic Algorithm, *Numerical Heat Transfer, Part A*, *46* (2004), 4, pp. 367-381

[36] Kim, K. W., Baek, S. W., Efficient Inverse Radiation Analysis in a Cylindrical Geometry Using a Combined Method of Hybrid Genetic Algorithm and Finite-Difference Newton Method, *JQSRT*, *108* (2007), 3, pp. 423-439

[37] Verma, S., Balaji, C., Multi-Parameter Estimation in Combined Conduction–Radiation from a Plane Parallel Participating Medium Using Genetic Algorithms, *Int. J. Heat Mass Transfer*, *50* (2007), 9-10, pp. 1706-1714

[38] Das, R., *et al.*, An Inverse Analysis of a Transient 2-D Conduction–Radiation Problem Using the Lattice Boltzmann Method and the Finite Volume Method Coupled with the Genetic Algorithm, *JQSRT*, *109* (2008), 11, pp. 2060-2077

[39] Qi, H., *et al.*, Inverse Radiation Analysis of a One-Dimensional Participating Slab by Stochastic Particle Swarm Optimizer Algorithm, *International Journal of Thermal Sciences*, *46* (2007), 7, pp. 649-661

[40] Qi, H., *et al.*, Application of Multi-Phase Particle Swarm Optimization Technique to Inverse Radiation Problem, *JQSRT*, *109* (2008), 3, pp. 476-493

[41] Lee, K. H., *et al.*, Inverse Radiation Analysis Using Repulsive Particle Swarm Optimization Algorithm, *Int. J. Heat Mass Transfer*, *51* (2008), 11-12, pp. 2772-2783

[42] Sun, Y. P., *et al.*, Estimating Soot Volume Fraction and Temperature in Flames Using Stochastic Particle Swarm Optimization Algorithm, *Int. J. Heat Mass Transfer*, *54* (2011), 1-3, pp. 217-224

[43] Modest, M. F., *Radiative Heat Transfer*, 2nd ed., Academic Press, Waltham, Mass., USA, 2003

[44] Lockwood, F. C., Shah, N. G., A New Radiation Solution Method for Incorporation in General Combustion Prediction Procedures, *Proceedings*, 18th Symposium (Int.) on Combustion, Waterlou, Ont., Canada, The Combustion Institute, Pittsburgh, Cal., USA, 1981, pp. 1405-1414
[45] Magel, H. C., *et al.*, Numerical Simulation of Utility Boilers with Advanced Combustion Technologies, *Proceedings*, 8th International Symposium on Transport Phenomena in Combustion, San Francisco, Cal., USA, 1995, pp. 1-12
[46] Knaus, H., *et al.*, Evaluation of the 3D-Furnace Simulation Code AIOLOS by Comparing CFD Predictions of Gas Compositions with In-Furnace Measurements in a 210 MW Coal-Fired Utility Boiler, *Progress in Computational Fluid Dynamics*, *1* (2001), 1-3, pp. 62-69

Paper submitted: June 21, 2013
Paper revised: March 9, 2014
Paper accepted: April 1, 2014